



University of
BRISTOL

UNIT LEAD: LUCIA MARUCCI

Minimal model for signal-induced Ca^{2+}
oscillations and for their frequency encoding
through protein phosphorylation: A critical
model comparison and dynamics analysis

Author
VEDANG JOSHI

Email
vedang.joshi.2018@bristol.ac.uk

1 Introduction

Many studies in the past decades have found that biological processes and intracellular structures (such as genes and proteins) display oscillatory behaviour [18]. We observe this phenomenon in heartbeats [7], respiration [23], and cell cycles [16]. On the cellular scale, this is evident in biochemical interactions involving calcium ions. The calcium ion (Ca^{2+}) plays a vital role in regulating heat production and facilitating intracellular communication [2].

In the cell, the Ca^{2+} concentrations are quite low ($\approx 100\text{nM}$) [10]. Thus, the influx of small quantities of Ca^{2+} from the endoplasmic reticulum (the largest intracellular store of Ca^{2+}) (ER) into the cytosol (fluid within the cell walls embedding the other organelles) causes rapid and reversible changes in the Ca^{2+} concentrations. These concentration changes manifest as oscillations. These oscillations are signalling mechanisms, carried by the oscillation frequency [28]. For instance, the oscillation frequency of Ca^{2+} is known to control the contraction of pulmonary and arteriole smooth muscles in the lungs [24] whilst increasing the efficiency of specific gene expression and cell differentiation [13]. Specific information can be encoded in this signal and transported through the cell without causing harm to the cell itself [4].

These oscillations are regulated by various mechanisms. The most common signalling pathway works as follows: the stimulation generated by the binding of a ligand-receptor on the cell wall activates a particular enzyme called phospholipase-C. This enzyme hydrolyses to create the inositol 1,4,5-trisphosphate (InsP_3) signalling molecule [22]. This InsP_3 molecule diffuses to the ER and binds to an InsP_3 -receptor. This receptor gets activated and acts as a channel to release Ca^{2+} from the ER into the cytosol [27] This mechanism is known as Ca^{2+} -induced Ca^{2+} release (CICR).

Berridge *et al.* [5] use this CICR mechanism to hypothesise that an external stimulus triggers the synthesis of a certain amount of InsP_3 . This, in turn, triggers the release of a particular amount of Ca^{2+} from an InsP_3 -sensitive pool. Goldbeter *et al.* [15] use this hypothesis to develop a minimal model for such signal-induced oscillations based on CICR. They give a system of ODEs, whose dynamics we solve and explore further in this paper. We first describe the biological model, as given by the authors. We then provide references to the literature, which demonstrate the variety of approaches in modelling Ca^{2+} oscillations. We then simulate the model numerically and conduct a phase plane analysis to study the dynam-

ics of this non-linear system. Finally, we conduct a bifurcation analysis using numerical continuation of this system of ODEs. We shall henceforth refer to this study by Goldbeter *et al.* as the ‘case study’, with the model referred to as the ‘case study model’ for brevity.

The tool of choice for the simulation and analysis of dynamical systems is the PyDSTools [11] toolbox in Python. This toolbox is chosen for its low-level integrators and continuation algorithms written in C, Python and Fortran, making the execution of such analyses extremely fast. The source code for the analyses and diagrams for this paper may be found at https://github.com/vedang-joshi/physio_medicine_cw.

2 Biological model

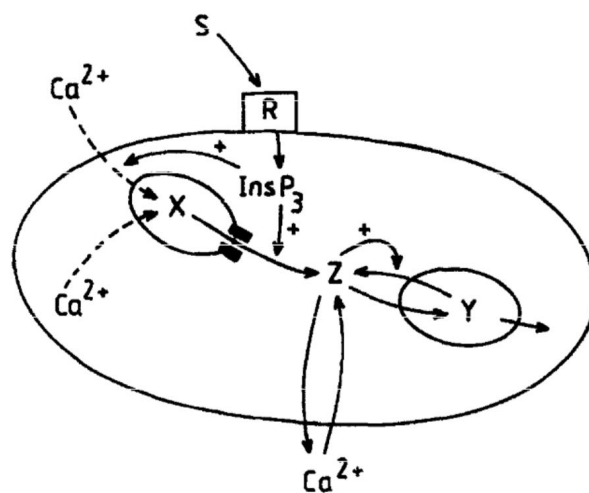


Figure 1: A graphical representation of the system. The stimulus (S) acts on the cell receptor (R). This triggers the synthesis of InsP_3 . This then triggers the release of Ca^{2+} in the InsP_3 -sensitive store (X) at a rate proportional to the saturation function β of the InsP_3 -receptor. Ca^{2+} in the cytosol (Z) is pumped into an InsP_3 -insensitive store (Y). Ca^{2+} in Y is released into the cytosol (i.e. in Z) by a process regulated by the cytosolic Ca^{2+} . Figure obtained from [14].

The Goldbeter model [15] that we are considering for further analysis is based off the CICR mechanism, as discussed earlier. The authors are primarily investigating whether the interactions between the InsP_3 -sensitive and InsP_3 -insensitive intracellular stores of

Ca^{2+} give rise to these oscillations in the Ca^{2+} concentrations in the cytosol.

To reiterate the CICR mechanism slightly, the system is based on the synthesis of InsP_3 based off an external stimulus on a cell receptor. This synthesis triggers the release of Ca^{2+} in the InsP_3 -sensitive store (X). The amount of Ca^{2+} released is controlled by the saturation function β of the InsP_3 -receptor. The Ca^{2+} in the cytosol (Z) is pumped into an InsP_3 -insensitive store (Y) and back into Z , creating a feedback loop. It is believed that this feedback loop structure gives rise to cytosolic Ca^{2+} oscillations [14]. The authors consider the dynamics only in Z and Y by assuming the release of Ca^{2+} in the InsP_3 -sensitive store to be an adjustable parameter [14]. See Figure 2 for a graphical representation of the problem.

Therefore the process may be modelled by the ODE system as follows [15]:

$$\frac{dZ}{dt} = v_0 + v_1\beta - v_2 + v_3 + k_f Y - kZ, \quad (1)$$

$$\frac{dY}{dt} = v_2 - v_3 - k_f Y, \quad (2)$$

where v_2 and v_3 are

$$v_2 = V_{M2} \frac{Z^n}{K_2^n + Z^n}, \quad (3)$$

$$v_3 = V_{M3} \frac{Y^m}{K_R^m + Y^m} \frac{Z^p}{K_A^p + Z^p}, \quad (4)$$

In equations 1 and 2, Z and Y represent the concentrations of free Ca^{2+} in the cytosol and the InsP_3 -insensitive stores respectively. The parameter v_0 denotes the constant extracellular input of Ca^{2+} . The parameter $v_1\beta$ refers to the InsP_3 -modulated release of Ca^{2+} from the InsP_3 -sensitive store. The variables v_2 and v_3 refer to the rate of pumping Ca^{2+} into the InsP_3 -insensitive stores and the rate of release of Ca^{2+} from that InsP_3 -insensitive store into the cytosol. The parameter k_f denotes the rate of passive leak of Y into Z . The rate of transport of cytosolic Ca^{2+} is linear, denoted by k .

The equations 3 and 4 allow for cooperativity in pumping, release and activation of Ca^{2+} . Here, the parameters n , m , p refer to the Hill coefficients categorising the processes of pumping, release and activation respectively. The parameters V_{M2} and V_{M3} are the maximum values of the rates v_2 and v_3 respectively. The parameters K_2 , K_R and K_A refer to the threshold constants for pumping, release and activation.

3 Related Works

There have been many mathematical models proposed for Ca^{2+} oscillations. The case study model assumes the existence of two pools for Ca^{2+} and emphasises the effect of CICR on Ca^{2+} oscillations. The model was proposed before important features of InsP_3 and Ca^{2+} -gated channel opening were known. The release of Ca^{2+} from intracellular pools may be mediated by either the InsP_3 -receptor or by the ryanodine receptor (RyR) [21]. It was found that both types of release channels were not required [21]. Here, we give a historical overview of the various models proposed for Ca^{2+} oscillations. We provide comparisons to other models in the literature for a thorough understanding of the biological processes involved and the progression of models over time.

Somogyi and Stucki [29] provide one of the first models for Ca^{2+} oscillations. They construct their model using a CICR framework, but assume only one single InsP_3 -sensitive pool exists. The authors restrict their analysis to oscillations in liver cells. They also restrict the passive flows of Ca^{2+} across the InsP_3 -sensitive channel and the two Ca^{2+} leaks to unidirectional fluxes only. This is a simplification of the model considered subsequently by the case study. The authors observe a mathematical similarity between the rate laws employed in their model and the well-established Brusselator system of equations, one of the first models capable of explaining the onset of stable oscillations.

The De Young-Keizer model [12] is similar to the case study model to the extent that both models are deterministic and consider external stimulus-induced Ca^{2+} oscillations. The authors construct a simplified model of the InsP_3 -receptor by assuming that three independent sub-units are responsible for the conduction of Ca^{2+} , where each sub-unit consists of an InsP_3 and two Ca^{2+} binding sites. One of these sites is for activation and the other for inhibition of Ca^{2+} . The case study assumes a single binding site and reports that an important property of the case study model is that recurrent Ca^{2+} oscillations may occur in the absence of InsP_3 oscillations [15]. This directly contradicts the findings by the De Young-Keizer model. The De Young-Keizer model shows that sustained InsP_3 oscillations are a product of a positive feedback mechanism of Ca^{2+} on InsP_3 production. This mechanism produces Ca^{2+} oscillations. The idea of a positive feedback mechanism of Ca^{2+} on InsP_3 production has been verified experimentally in many subsequent studies [30, 3]. The lack of incorporation of this positive feedback mechanism of Ca^{2+}

on InsP_3 production is one of the fundamental limitations of the case study model. The De Young-Keizer model also assumes that ligands may bind to any unoccupied site on receptor irrespective of whether the other sites are InsP_3 or Ca^{2+} binding sites.

Atri *et. al.* [1] developed a model for Ca^{2+} based off a single gating system. They use a De Young-Keizer framework for the InsP_3 -receptor but separate the Ca^{2+} sites as positive and negative regulatory sites (an InsP_3 site, a positive and negative regulatory Ca^{2+} site). The binding of regulatory factors (eg. ligands) is still assumed to be state independent, as with the De Young-Keizer model. The main assumption in the Atri model is that the negative Ca^{2+} regulatory site requires a cooperative binding of two Ca^{2+} to close the channel. For brevity, we do not include the system of ODEs proposed by Atri *et. al.* Instead, we provide a short review of the similarities in the construction of the case study model and the Atri *et. al.* model. Both models assume a constant rate of Ca^{2+} influx from the exterior of the cell into the cytosol (represented by v_0 and β in the case study and Atri models respectively). Both models also consider a constant concentration of InsP_3 at which oscillations occur. Yet, the modelling of the Ca^{2+} flux in such a manner resembles a simplified version of the De Young-Keizer model [1] and only assumes a single pool of Ca^{2+} , as opposed to two pools in the case study model. Thus, the model creates a link between the models of Ca^{2+} which may or may not require oscillating InsP_3 to drive Ca^{2+} oscillations.

For all the models considered above, the limiting process was the Ca^{2+} exchange with the extracellular medium. Li & Rinzel [21] analysed the nine variable De Young-Keizer model and reduce it to a two-variable system. The authors consider the limiting process here to be the InsP_3 -receptor desensitisation. The authors analyse the time scales of the three channel gating process (namely the InsP_3 regulation, Ca^{2+} activation and inactivation) in this revised model of the De Young-Keizer model. The authors conducted a bifurcation analysis of this reduced system and found the bifurcation diagram to be qualitatively identical to the one constructed using the De Young-Keizer model. The authors compare the reduced model to the Hodgkin-Huxley formalism for ER membrane electrical excitability.

More recently, Lavrentovich and Hemkin [20] used a CICR framework to model spontaneous Ca^{2+} oscillations in astrocytes. Astrocytes are a fundamental structural element holding neurons together and

play an active part in the signalling process [9]. This model closely resembles the case study model by considering the dynamics of the Ca^{2+} concentration in the ER (Y), and the InsP_3 concentration in the cell (Z). In this model, the oscillatory behaviour is initiated by small changes in cytosolic Ca^{2+} , caused by varying the extracellular Ca^{2+} flux across the plasma membrane into the cytosol. The two pool model qualitatively demonstrates the same dynamics across different cells, thereby validating the case study model.

To determine the exact conditions necessary for oscillations, intuition is insufficient. To establish a set of requirements, a stability analysis is necessary. An advantage of the models discussed above is that the temporal changes can be analytically derived. We shall discuss this further in the next section.

4 Temporal Dynamics Analysis

This section is devoted to demonstrating the influence of the various parameters in the system, on the long-term observed dynamics in the case study model. We start by reproducing the plot for the temporal dynamics in [14] (see Figure 2). We observe sustained oscillations in cytosolic Ca^{2+} with a period of the order 1. We shall vary certain parameters in the case study system of ODEs, whilst also providing some reasoning as to why and how a particular parameter was chosen and varied.

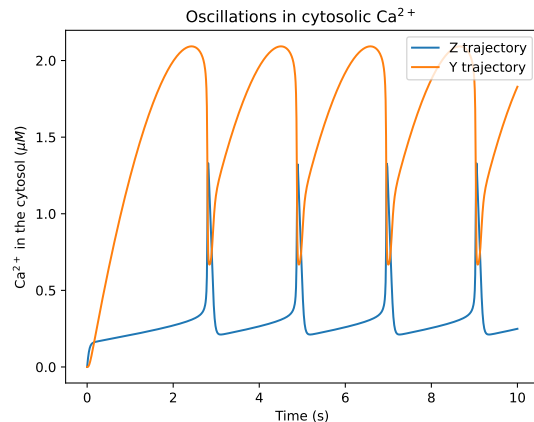


Figure 2: Oscillations in cytosolic Ca^{2+} . Reproduction of Figure 2 in [14]. Curves obtained by numerical integration of the equations 1 and 2, using the following parameter values: $v_0 = 1\mu M s^{-1}$, $k = 10s^{-1}$, $k_f = 1s^{-1}$, $v_1 = 7.3\mu M s^{-1}$, $V_{M2} = 65\mu M s^{-1}$, $V_{M3} = 500\mu M s^{-1}$, $K_2 = 1\mu M$, $K_R = 2\mu M$, $K_A = 0.9\mu M$, $m = n = 2$, $p = 4$, $\beta = 0.301$. Initial conditions: $Z = 0\mu M$, $Y = 0\mu M$.

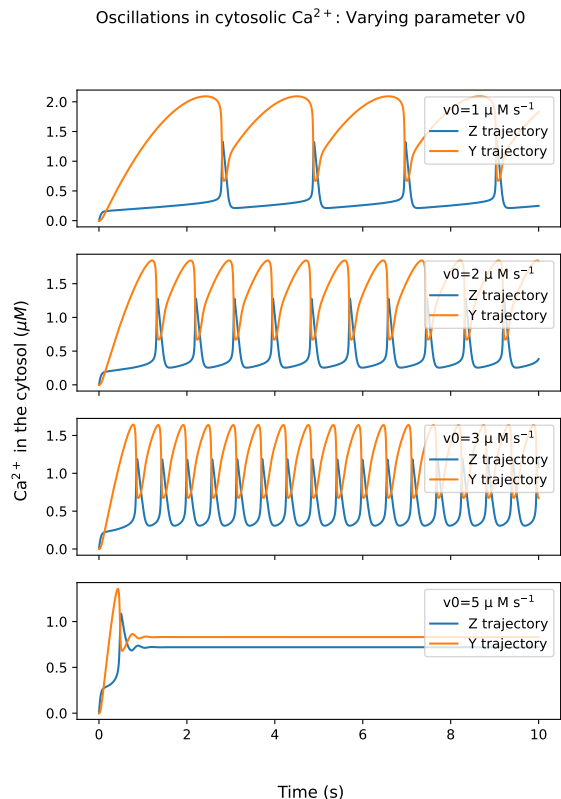


Figure 3: Change in period of oscillations in cytosolic Ca^{2+} by varying v_0 . The top figure is a reproduction of Figure 2, with the next three figures showing incremental variations in v_0 . $v_0 = 1, 2, 3, 5 \mu\text{M s}^{-1}$ respectively for the four figures (from top to bottom panels). The rest of the system parameter values are as given in Figure 2.

We know that histamine (nitrogenous compound involved localised immune system responses) causes the influx of Ca^{2+} via voltage-gated calcium channels in certain cell membranes [25]. It has been demonstrated that low doses of histamine causes repetitive spikes in Ca^{2+} , whereas higher doses of histamine cause a maintained high level of Ca^{2+} [17]. This indicates that varying the levels of external Ca^{2+} (v_0) would result in fundamental characteristic changes in the dynamics of the case study system of ODEs. To this end, we keep the other parameter values constant as seen in Figure 2 and only vary v_0 (see Figure 3). We observe that there is a threshold value for v_0 $3 \mu\text{M s}^{-1} < v_0 < 5 \mu\text{M s}^{-1}$ where sustained oscillations cease to exist. Only a maintained constant level of cytosolic Ca^{2+} is observed. These observations are consistent with the claim by Jacob *et. al.* [17] as mentioned before. We may conclude that the external influx of Ca^{2+} is one of the key parameters

in driving CICR based oscillations.

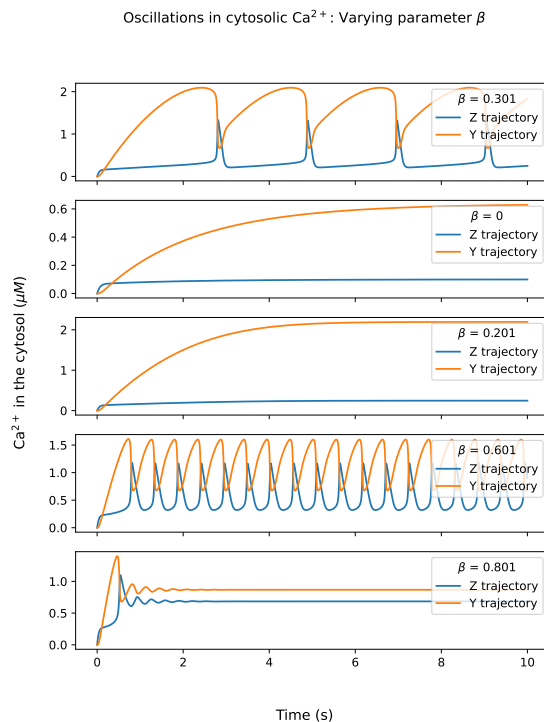


Figure 4: Change in period of oscillations in cytosolic Ca^{2+} by varying β . The top figure is a reproduction of Figure 2, with the next four figures showing slight variations in β . $\beta = 0.301, 0, 0.201, 0.601, 0.801$ respectively for the five figures (from top to bottom panels). The rest of the system parameter values are as given in Figure 2.

When the case study model was published, a widely held view was that Ca^{2+} oscillations are driven only by InsP_3 oscillations. This claim was proposed, in part, due to the fact that InsP_3 controls a constant flow of Ca^{2+} into the cytosol regulated by the rate β . We reproduce the results from the case study [14] and back up the authors' views that there exist a range of rate values $0.201 < \beta < 0.801$ (a stricter bounding $0.291 < \beta < 0.775$ is given in [14]), where Ca^{2+} oscillations occur (see Figure 4). The authors in the case study also remark that the constant input from InsP_3 -sensitive Ca^{2+} stores cannot be replenished for all time, so reducing the β parameter to zero should theoretically suppress all oscillations. We show this to be the case by setting $\beta = 0$ (see the second panel from the top in Figure 4). This indicates that the constant input of Ca^{2+} into the cytosol triggered by the external signal, forms part of a key driving mechanism for Ca^{2+} cytosolic oscillations.

The influence of the above two variables (i.e. v_0 and β) were considered by the authors in the case study, and we successfully reproduced and qualitatively backed the authors' claims of the processes surrounding Ca^{2+} cytosolic oscillations. Yet, the obvious influence of the intracellular pumping and Ca^{2+} release (governed by V_{M2} and V_{M3}) has not been talked about at all in the case study.

We aim to fill this gap in the analysis here. We vary the maximum rate of Ca^{2+} pumping in intracellular store (V_{M2}) and obtain bounds between which sustained oscillations of cytosolic Ca^{2+} may be observed. We find that sustained oscillations exist for the parameter values given in Figure 2, for $59 \mu\text{M}s^{-1} < V_{M2} < 145 \mu\text{M}s^{-1}$ (see Figure 5). A steady state is reached for values of V_{M2} outside this range. We note that for $59 \mu\text{M}s^{-1} < V_{M2} < 145 \mu\text{M}s^{-1}$, there appears to be a linear relationship between the maximum Z amplitude and the values of V_{M2} . So, for higher values of V_{M2} , we see higher amplitudes, resulting in a theoretical increase in the energy of the system. We also observe that the increase of V_{M2} results in an increase in the frequency of oscillations.

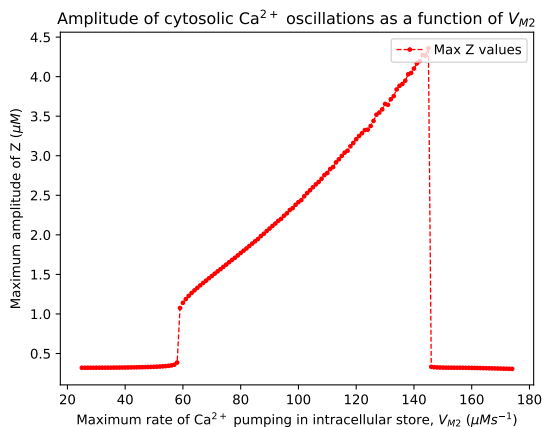


Figure 5: Amplitude of cytosolic Ca^{2+} oscillations as a function of V_{M2} . For the values of the other parameters given in Figure 2, sustained Ca^{2+} oscillations are observed when $59 \mu\text{M}s^{-1} < V_{M2} < 145 \mu\text{M}s^{-1}$. Points in red denote the maximum value of the trajectories obtained by numerical integration of Equations 1 and 2.

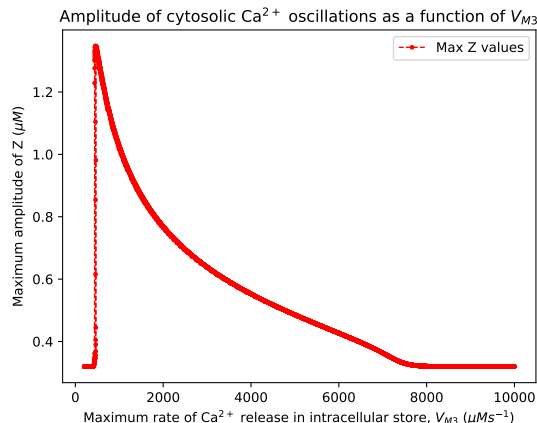


Figure 6: Amplitude of cytosolic Ca^{2+} oscillations as a function of V_{M2} . For the values of the other parameters given in Figure 2, sustained Ca^{2+} oscillations are observed when $438 \mu\text{M}s^{-1} < V_{M3} < 8450 \mu\text{M}s^{-1}$. Points in red denote the maximum value of the trajectories obtained by numerical integration of Equations 1 and 2.

We conduct a similar analysis for the maximum rate of Ca^{2+} release in the intracellular store (V_{M3}), and find that sustained oscillations exist for the parameter values as given in Figure 2, for $438 \mu\text{M}s^{-1} < V_{M3} < 8450 \mu\text{M}s^{-1}$ (see Figure 6). A steady state is reached for values of V_{M3} outside this range with oscillations in finite time, and then plateauing of the trajectories occurs.

5 Phase plane analysis

For most non-linear systems, it is impossible to find closed analytical solutions due to the influence of small changes of system parameters on the system dynamics. This necessitates the development of phase plane diagrams to determine qualitative features of the non-linear system. The approach here is largely pictorial, which helps visualise the behaviour of the system easily. From ideas in vector calculus, we know that every point (x, y) in the solution plane can be assigned a vector which does not change with time. A solution curve passing through (x, y) must have these zero time derivative vectors as its tangents. A collection of these vectors defines a vector field, and is used to qualitatively sketch a family of solution curves to the ODE system.

Instead of choosing arbitrary points for which to plot these zero derivative vectors, we compute the locus of points where the first time derivative of the system

of ODEs is zero (i.e. in the case study model, where $\dot{Z} = \dot{Y} = 0$). The set of points satisfying these respective rules is termed a nullcline (specifically Z and Y nullclines respectively in our case study model). Nullclines, therefore, separate the phase plane into regions of same-direction flow. At the intersection of these nullclines, the time derivative is zero in all directions in the plane and the system achieves equilibrium. From numerical integration of the Z and Y variables, we see that the trajectories settle to self-sustained oscillations for the parameter values given (see Figure 2 for reference). The occurrence of sustained oscillations requires a stable limit cycle in the system. A limit cycle is a closed trajectory in the phase space where states are visited and re-visited, repetitively. The existence of an equilibrium point within a limit cycle demonstrates the stability of the system.

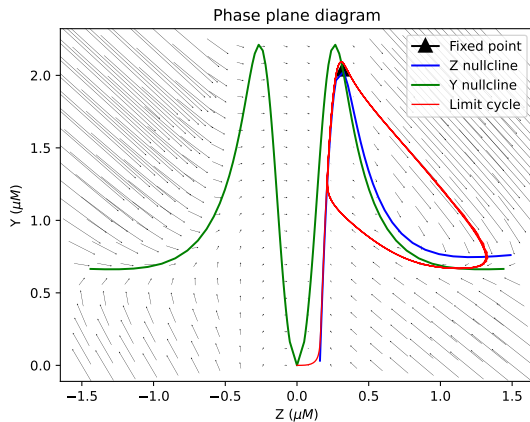


Figure 7: Phase plane diagram. The black triangle denotes the fixed point. The solid lines in blue and green denote the Z and Y nullclines respectively. The solid red line denotes the limit cycle generated from the trajectories obtained by numerical integration of Equations 1 and 2 for the parameter values given in Figure 2.

We shall also consider varying the parameters as shown in Section 4, within the individual ranges where sustained oscillations have been observed. We will use the results obtained by the case study authors along with our own analysis to determine the new parameter set values. We will show that a new set of parameters may not demonstrate oscillations, even if certain parameter values may demonstrate oscillations in the system individually. We will thus aim to highlight the non-trivial dynamics in this system of ODEs through a phase plane framework.

We compute the nullclines for the case study model for the parameter values as given in Figure 2, and also plot the equilibrium point which exists at $(Z = 0.32$ (2 d.p), $Y = 2.04$ (2 d.p)). We demonstrate the existence of a limit cycle and that the equilibrium point lies at the intersection of the nullclines within the limit cycle (see Figure 7), thus confirming the stability of the system. This also gives qualitative backing to the self-sustained oscillations observed in plotting the trajectories of Z and Y in finite time. By commencing the trajectory plots from the origin of the (Z, Y) phase space, we see that the trajectories keep visiting and revisiting the same neighbourhood around the equilibrium. We compute the eigenvalues of the Jacobian at this point and so we can characterise this equilibrium point as a stable centre.

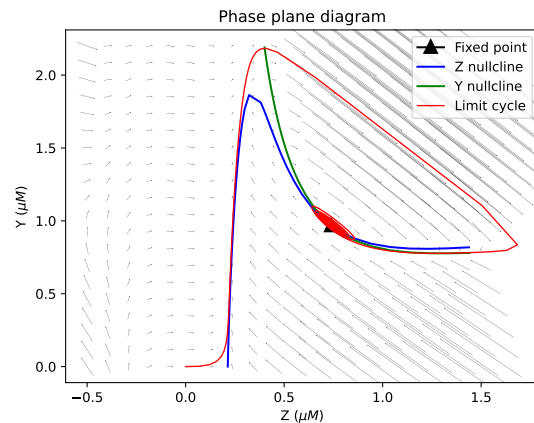


Figure 8: Phase plane diagram. The black triangle denotes the fixed point. The solid lines in blue and green denote the Z and Y nullclines respectively. The solid red line denotes the trajectories obtained by numerical integration of Equations 1 and 2 for the parameter values $v_0 = 3 \mu M s^{-1}$, $\beta = 0.601$, $V_{M2} = 120 \mu M s^{-1}$ and $V_{M3} = 700 \mu M s^{-1}$ and the other parameter values as given in Figure 2.

We perturb the system for the parameters v_0 , β , V_{M2} and V_{M3} , for values in the range, $1 \mu M s^{-1} < v_0 < 5 \mu M s^{-1}$, $0.291 < \beta < 0.775$, $59 \mu M s^{-1} < V_{M2} < 145 \mu M s^{-1}$, $59 \mu M s^{-1} < V_{M3} < 145 \mu M s^{-1}$. All parameters which were individually perturbed within these ranges have resulted in sustained oscillations being observed. We compute the fixed point for this new system to be $(Z = 0.74$ (2 d.p), $Y = 0.97$ (2 d.p)). Through computing the eigenvalues for the Jacobian for this new system, we discover that the slight perturbations result in the system exhibiting an asymptotically stable spiral. Importantly, the loss

of the limit cycle suggests that sustained oscillations can no longer be observed in the new system. Figure 8 shows this system with $v_0 = 3 \mu M s^{-1}$, $\beta = 0.601$, $V_{M2} = 120 \mu M s^{-1}$ and $V_{M3} = 700 \mu M s^{-1}$, with all other parameters kept the same as in Figure 2.

Through this phase portrait, we show that initially a small rise in the influx of free cytosolic Ca^{2+} results in a sharp rise in InsP₃-insensitive stores, but, with continuous rises in cytosolic Ca^{2+} , there is a gradual decline of InsP₃-sensitive stores until the system starts to spiral around a stable attractor at the equilibrium point (i.e. the system starts to oscillate with a high frequency around an equilibrium). We also note the clockwise direction of rotation of the system from both phase plane diagrams.

To present a complete analysis of system behaviour, we consider perturbing the system for the other parameters K_2 , K_R and K_A which influence the equations 3 and 4 - i.e. the cooperativity equations for the pumping, release and activation of Ca^{2+} . We vary these parameters as they are the threshold constants for the pumping, release and activation of Ca^{2+} , and would provide a complete overview as to how the system dynamics change with varying v_2 and v_3 . We consider a slight variation to the values of these parameters as given by the case study authors and propose new parameter values governed by physiological experimental evidence [8]. We set $K_2 = 0.6 \mu M$, $K_R = 13 \mu M$, $K_A = 0.4 \mu M$, with all other parameter values as given in Figure 2, and demonstrate that a limit cycle exists for this new set of parameters too, with the equilibrium point lying within the cycle (see Figure 9).

The phase plane diagram demonstrates that sustained oscillations are viewed in the system, even with large perturbation of threshold constants for the activation, release and pumping of Ca^{2+} . We find the fixed point to be at ($Z = 0.32$ (2 d.p), $Y = 3.67$ (2 d.p)), and, as the limit cycle is formed around this fixed point, we characterise this equilibrium point as stable. On comparing the Figures 8 and 9, we note that the change in the threshold constants allows the system to converge to the equilibrium state faster than varying the extracellular input of Ca^{2+} , the InsP₃ regulated release of Ca^{2+} and the maximum rates of equations governing the activation, release and pumping of intracellular Ca^{2+} . This obviously indicates that the feedback loop of pumping and release of Ca^{2+} drives the system dynamics rather than the threshold values of the pumping, activation and release of Ca^{2+} .

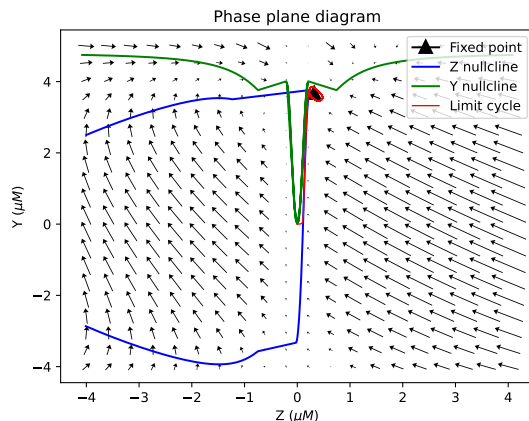


Figure 9: Phase plane diagram. The black triangle denotes the fixed point. The solid lines in blue and green denote the Z and Y nullclines respectively. The solid red line denotes the limit cycle generated from the trajectories obtained by numerical integration of Equations 1 and 2 for the parameter values $K_2 = 0.6 \mu M$, $K_R = 13 \mu M$, $K_A = 0.4 \mu M$ and the other parameter values as given in Figure 2.

6 Bifurcation analysis

For a thorough analysis of the biological systems, it is necessary to analyse the dependence of frequency and amplitude of oscillations on certain parameters. A simple method is to numerically integrate the system for different parameter sets and observe the system dynamics. This is the approach taken in the last few sections. However if we wish to conduct such an analysis on multiple parameters using various parameter values, this approach is quite tedious. A more systematic approach is the analysis of the neighbourhood of bifurcations from the stable steady states, which leads to oscillations in the system. In the last section, we shall introduce the ideas behind bifurcation analysis. We shall explore the bifurcations and bifurcation points observed in the case study model and explain how the dynamics of the system depend on the β parameter i.e. the saturation function of the InsP₃ receptor.

In all models considered above, we note that the oscillations occur due to the existence of fast and slow processes. To reiterate, if the Ca^{2+} channel is open, then the Ca^{2+} release rate is faster than the pump rate. Such oscillations are termed 'relaxation oscillations'. Generally in relaxation oscillations, the concentration gradient slowly builds across the ER and is then dissipated in a sudden discharge. The slow

buildup is represented as the phase between spikes and the dissipation occurs during the first part of the spike i.e. the sharp upstroke (see the Z trajectory in Figure 2)

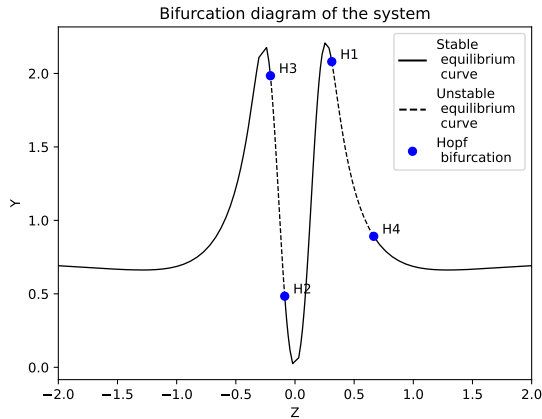


Figure 10: Bifurcation diagram of the system. The solid line in black denotes the stable equilibrium curve. The dotted black line denotes the unstable equilibrium curve. The blue dots show the Hopf bifurcations in the system. This analysis is conducted for the system of equations 1 and 2 for the parameter values as given in Figure 2.

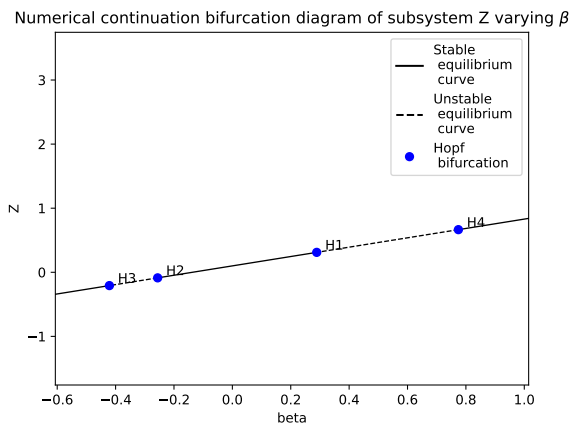


Figure 11: Bifurcation diagram of the Z subsystem varying β . The solid line in black denotes the stable equilibrium curve. The dotted black line denotes the unstable equilibrium curve. The blue dots show the Hopf bifurcations in the system. This analysis is conducted for the system of equations 1 and 2 for the parameter values as given in Figure 2.

Bifurcations occur if the system contains dynamics in

the neighbourhood of certain parameter values which topologically differ from the system dynamics at these parameter values [6]. Across the models considered so far in the literature review (including the case study model), the most frequent transition which leads to self-sustained oscillations in Ca^{2+} is the Hopf bifurcation. Hopf bifurcations are solely characteristic of non-linear systems. If the phase trajectory of a system converges to a focus for a certain set of parameters, and small changes to the parameter values results in the focus converging to a closed curve, then a Hopf bifurcation is said to have occurred. We observe this behaviour during the phase plane analysis (see Figures 7 and 8). Mathematically speaking, a system undergoes a Hopf bifurcation if the fixed point in the system loses stability as a pair of complex conjugate eigenvalues crosses the complex imaginary axis. In relaxation oscillations, the growth of the oscillation amplitude in the neighbourhood of the Hopf bifurcation, occurs at an extremely small parameter range [26], which is why we study this behaviour. Let us illustrate these ideas further.

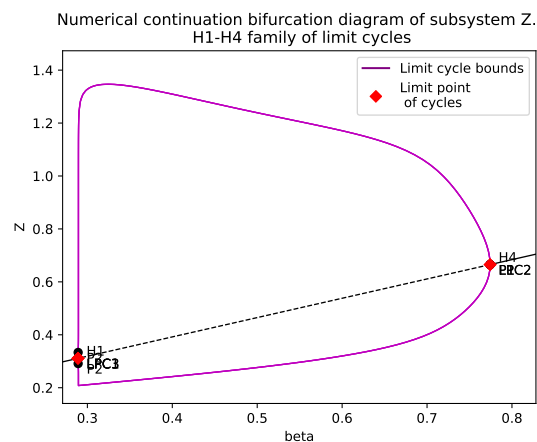


Figure 12: Numerical continuation of the Z subsystem varying β focusing on the H1-H4 family of limit cycles. The solid purple line denotes the maximum and minimum values of Z on limit cycles. The red diamond denotes the limit point of cycles bifurcation as we track the limit cycle originated from the bifurcations H1 and H4.

PyDSTools contains an inbuilt Moore-Penrose numerical continuation method, which we apply to the case study model and obtain the equilibrium point curve. We retain the original parameter values as given in Figure 2. We identify four Hopf bifurcations in the system labelled H1, H2, H3 and H4 (see Figure 10). The solid black line shows the stable

equilibrium curve and the dotted black line shows the unstable equilibrium curve. We prepare the system to start close to the steady state with $\beta = 1$, $Z = 0.5$, $Y = 2$. We consider β to be the free parameters henceforth in our analysis. We observe that the equilibrium loses its stability at H3, regains it from H2 through to H1 and loses it between H1 and H4. It is necessary to analyse what happens at each of these individual Hopf bifurcations. This analysis includes categorising these bifurcations as subcritical or supercritical. Whether a Hopf bifurcation is supercritical or subcritical is determined by the sign of the first Lyapunov coefficient (l_1) of the dynamical system near the equilibrium [19]. When $l_1 < 0$, the Hopf bifurcation is supercritical and for $l_1 > 0$, the Hopf bifurcation is subcritical [31].

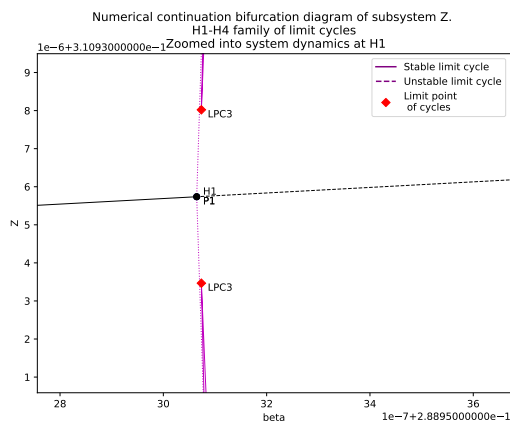


Figure 13: Numerical continuation of the Z subsystem varying β focusing on the H1-H4 family of limit cycles. System dynamics at H1. The solid purple line denotes the stable limit cycle. The dotted purple line denotes the unstable limit cycle. The red diamond denotes the limit point of cycles bifurcation as we track the limit cycle originated from the bifurcations H1 and H4.

For the system of ODEs in Equations 1 and 2, H1 was identified at $\beta = 0.29$, $Z = 0.31$, $Y = 2.08$ (2 d.p) with eigenvalues $\lambda = -0.000001 \pm 5.18i$. We compute $l_1 = 166.31$ (2 d.p), so we characterise H1 as a subcritical Hopf bifurcation. H2 was identified at $\beta = -0.26$, $Z = -0.09$, $Y = 0.48$ (2 d.p) with eigenvalues $\lambda = \pm 3.18i$. We compute $l_1 = -21.46$ (2 d.p), so we characterise H2 as a supercritical Hopf bifurcation. H3 was identified at $\beta = -0.42$, $Z = -0.21$, $Y = 1.98$ (2 d.p) with eigenvalues $\lambda = \pm 3.68i$. We compute $l_1 = -193.32$ (2 d.p), so we characterise H3 as a supercritical Hopf bifurcation. H4 was identified at $\beta = 0.77$, $Z = 0.66$, $Y = 0.89$ (2 d.p) with

eigenvalues $\lambda = \pm 19.14i$. We compute $l_1 = -269.19$ (2 d.p), so we characterise H4 as a supercritical Hopf bifurcation.

For deeper understanding of the system behaviour, we shall constrain our analysis to the Z subsystem while varying the parameter β (Figure 11). This is because the Z subsystem implicitly depends on the Y subsystem behaviour. Immediately we note, though mathematically allowed, analysing this subsystem with negative β values has no physiological meaning. The case study authors set β to control the release of Ca^{2+} from the InsP_3 -sensitive stores. This implies the direction of flow is predetermined: β must always be positive. We further constrain our Z subsystem dynamics where $\beta > 0$.

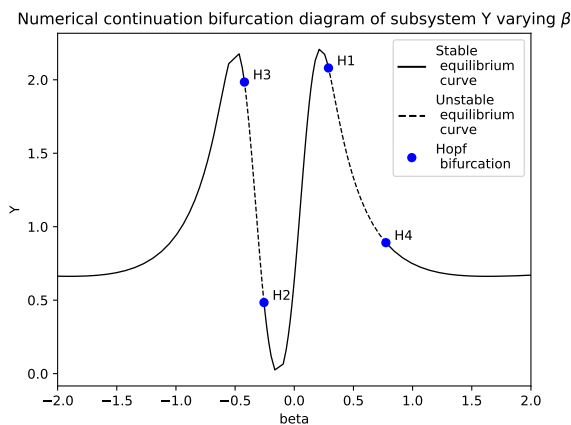


Figure 14: Bifurcation diagram of the Y subsystem varying β . The solid line in black denotes the stable equilibrium curve. The dotted black line denotes the unstable equilibrium curve. The blue dots show the Hopf bifurcations in the system. This analysis is conducted for the system of equations 1 and 2 for the parameter values as given in Figure 2.

We track the limit cycles arising from the Hopf bifurcations using numerical continuation. We found two distinct families of limit cycles originating from the four Hopf bifurcation points in the Z subsystem. The maximum and minimum values of these limit cycles are plotted as a solid purple line. As discussed earlier, we may disregard the H2-H3 family of limit cycles, as they lie in the regions where $\beta < 0$. For the H1-H4 family of limit cycles, we obtain three limit point of cycles LPC1, LPC2, LPC3 (Figure 12). We observe that oscillations appear and disappear in Hopf bifurcations as β increases. Figure 13 shows the system dynamics close to H1. We observe a subcritical bifurcation at H1, which leads to a branch of unstable

limit cycles. These turn around in a saddle-node of periodic orbits bifurcation to give a branch of stable limit cycles. We note that this analysis agrees with the temporal dynamics analysis where we vary β , as the limit cycles only exist when $\approx 0.3 < \beta < \approx 0.8$ which agrees with [14]. We identify the H1-H4 family of limit cycles as the drivers behind the Z subsystem oscillations, i.e. the subsystem where the oscillations arise from the cytosolic Ca^{2+} being pumped into an InsP_3 -insensitive store. This effectively suggests that the H1-H4 family of limit cycles drives the oscillations in the entire system as given in equations 1 and 2.

Although we have discussed that the Z subsystem analysis completely examines the Y subsystem dynamics, for comprehensiveness in our analysis, we verify our discussion through a brief analysis of the Y subsystem dynamics. Figure 14 shows the bifurcation diagram of the Y subsystem varying β . Through a similar argument as observed for the Z subsystem dynamics, for the H1-H4 family of limit cycles, we obtain three limit point of cycles LPC2, LPC3 (Figure 15). We employ the same technique as before, and observe the dynamics close to the H1 bifurcation and conclude that there are unstable limit cycles turning into stable limit cycles through a saddle-node of periodic orbits bifurcation (Figure 16).

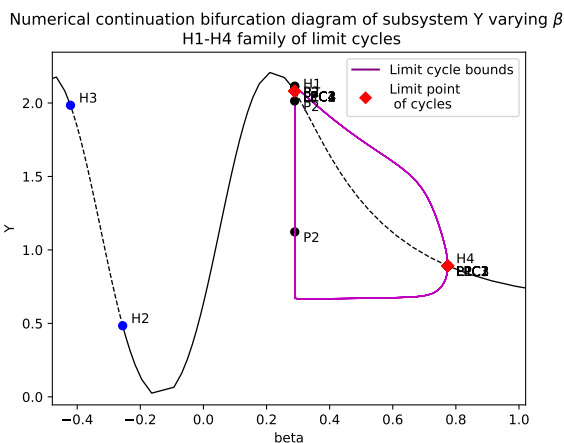


Figure 15: Numerical continuation of the Y subsystem varying β focusing on the H1-H4 family of limit cycles. The solid purple line denotes the maximum and minimum values of Y on limit cycles. The red diamond denotes the limit point of cycles bifurcation as we track the limit cycle originated from the bifurcations H1 and H4.

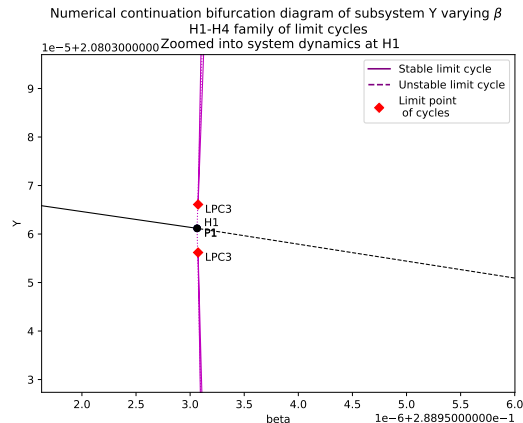


Figure 16: Numerical continuation of the Y subsystem varying β focusing on the H1-H4 family of limit cycles. System dynamics at H1. The solid purple line denotes the stable limit cycle. The dotted purple line denotes the unstable limit cycle. The red diamond denotes the limit point of cycles bifurcation as we track the limit cycle originated from the bifurcations H1 and H4.

We have comprehensively discussed the bifurcation diagram in terms of β , by breaking down the case study model into individual subsystems and applying numerical continuation effectively.

Bibliography

- [1] ATRI, A., AMUNDSON, J., CLAPHAM, D., AND SNEYD, J. A single-pool model for intracellular calcium oscillations and waves in the xenopus laevis oocyte. *Biophysical Journal* 65, 4 (1993), 1727–1739.
- [2] BERRIDGE, M. J. Neuronal calcium signaling. *Neuron* 21, 1 (1998), 13–26.
- [3] BERRIDGE, M. J. Inositol trisphosphate and calcium signalling mechanisms. *Biochimica et Biophysica Acta (BBA)-Molecular Cell Research* 1793, 6 (2009), 933–940.
- [4] BERRIDGE, M. J., BOOTMAN, M. D., AND LIPP, P. Calcium—a life and death signal. *Nature* 395, 6703 (1998), 645–648.
- [5] BERRIDGE, M. J., COBBOLD, P., AND CUTHBERTSON, K. Spatial and temporal aspects of cell signalling. *Philosophical Transactions of the Royal Society of London. B, Biological Sciences* 320, 1199 (1988), 325–343.
- [6] BLYTH, M., RENSON, L., AND MARUCCI, L. Tutorial of numerical continuation and bifurcation theory for systems and synthetic biology. *arXiv preprint arXiv:2008.05226* (2020).
- [7] BROWN, H., DIFRANCESCO, D., AND NOBLE, S. Cardiac pacemaker oscillation and its modulation by autonomic transmitters. *Journal of Experimental Biology* 81, 1 (1979), 175–204.
- [8] CARAFOLI, E., AND CROMPTON, M. The regulation of intracellular calcium. *Elsevier* 10 (1978), 151–216.
- [9] CHARLES, A. C., MERRILL, J. E., DIRKSEN, E. R., AND SANDERSON, M. J. Intercellular signaling in glial cells: calcium waves and oscillations in response to mechanical stimulation and glutamate. *Neuron* 6, 6 (1991), 983–992.
- [10] CLAPHAM, D. E. Calcium signaling. *Cell* 131, 6 (2007), 1047–1058.
- [11] CLEWLEY, R. H., SHERWOOD, W., LAMAR, M., AND GUCKENHEIMER, J. Pydstool, a software environment for dynamical systems modeling. URL <http://pydstool.sourceforge.net> (2007).
- [12] DE YOUNG, G. W., AND KEIZER, J. A single-pool inositol 1, 4, 5-trisphosphate-receptor-based model for agonist-stimulated oscillations in ca_{2+} concentration. *Proceedings of the National Academy of Sciences* 89, 20 (1992), 9895–9899.
- [13] DOLMETSCH, R. E., XU, K., AND LEWIS, R. S. Calcium oscillations increase the efficiency and specificity of gene expression. *Nature* 392, 6679 (1998), 933–936.
- [14] DUPONT, G., BERRIDGE, M., AND GOLDBETER, A. Signal-induced ca_{2+} oscillations: properties of a model based on ca_{2+} -induced ca_{2+} release. *Cell calcium* 12, 2-3 (1991), 73–85.
- [15] GOLDBETER, A., DUPONT, G., AND BERRIDGE, M. J. Minimal model for signal-induced ca_{2+} oscillations and for their frequency encoding through protein phosphorylation. *Proceedings of the National Academy of Sciences* 87, 4 (1990), 1461–1465.
- [16] HARTWELL, L. H., AND KASTAN, M. B. Cell cycle control and cancer. *Science* 266, 5192 (1994), 1821–1828.
- [17] JACOB, R., MERRITT, J. E., HALLAM, T. J., AND RINK, T. J. Repetitive spikes in cytoplasmic calcium evoked by histamine in human endothelial cells. *Nature* 335, 6185 (1988), 40–45.
- [18] KRUSE, K., AND JÜLICHER, F. Oscillations in cell biology. *Current opinion in cell biology* 17, 1 (2005), 20–26.
- [19] KUZNETSOV, Y. Andronov-hopf bifurcation. *Scholarpedia* 1, 10 (2006), 1858.
- [20] LAVRENTOVICH, M., AND HEMKIN, S. A mathematical model of spontaneous calcium (ii) oscillations in astrocytes. *Journal of Theoretical Biology* 251, 4 (2008), 553–560.
- [21] LI, Y.-X., AND RINZEL, J. Equations for $insp3$ receptor-mediated $[ca_{2+}]_i$ oscillations derived from a detailed kinetic model: a Hodgkin-Huxley like formalism. *Journal of theoretical Biology* 166, 4 (1994), 461–473.
- [22] MIKOSHIBA, K. The $insp3$ receptor and intracellular ca_{2+} signaling. *Current opinion in neurobiology* 7, 3 (1997), 339–345.
- [23] PAYDARFAR, D., AND ELDRIDGE, F. L. Phase resetting and dysrhythmic responses of the respiratory oscillator. *American Journal of Physiology-Regulatory, Integrative and Comparative Physiology* 252, 1 (1987), R55–R62.

- [24] PEREZ, J. F., AND SANDERSON, M. J. The frequency of calcium oscillations induced by 5-HT, acetylcholine, and potassium determine the contraction of smooth muscle cells of intrapulmonary bronchioles. *The Journal of general physiology* 125, 6 (2005), 535–553.
- [25] PFANZAGL, B., ZEVALLOS, V. F., SCHUPPAN, D., PFRAGNER, R., AND JENSEN-JAROLIM, E. Histamine causes influx via t-type voltage-gated calcium channels in an enterochromaffin tumor cell line: potential therapeutic target in adverse food reactions. *American Journal of Physiology-Gastrointestinal and Liver Physiology* 316, 2 (2019), G291–G303.
- [26] SCHUSTER, S., MARHL, M., AND HÖFER, T. Modelling of simple and complex calcium oscillations: From single-cell responses to intercellular signalling. *European Journal of Biochemistry* 269, 5 (2002), 1333–1355.
- [27] SNEYD, J. Models of calcium dynamics. *Scholarpedia* 2, 3 (2007), 1576.
- [28] SNEYD, J., HAN, J. M., WANG, L., CHEN, J., YANG, X., TANIMURA, A., SANDERSON, M. J., KIRK, V., AND YULE, D. I. On the dynamical structure of calcium oscillations. *Proceedings of the National Academy of Sciences* 114, 7 (2017), 1456–1461.
- [29] SOMOGYI, R., AND STUCKI, J. Hormone-induced calcium oscillations in liver cells can be explained by a simple one pool model. *Journal of biological chemistry* 266, 17 (1991), 11068–11077.
- [30] WANG, S., AND THOMPSON, S. H. Local positive feedback by calcium in the propagation of intracellular calcium waves. *Biophysical journal* 69, 5 (1995), 1683–1697.
- [31] YAN, Z. Hopf bifurcation in the Lorenz-type chaotic system. *Chaos, Solitons & Fractals* 31, 5 (2007), 1135–1142.